about 2,600 yr (an average of events *a–f* Fig. 1) elapsing between the bottom water and surface circulation changes and 3,000 yr between the change in surface circulation and the recession of the continental glaciers. Because of the relatively wide spacing in time of individual samples from Y69-106P (the average sample interval is about 4,000 yr) these estimates represent maximum lag times.

If the lags between the carbonate and opal accumulation rate curves were random and independent, the probability of the observed succession in the six events *a–f* in Fig. 1 would be 0.016—highly unlikely. Rather, the observed changes seem to be systematic and are consistent with two recent models[8,13] of climatic change. Newell[8] has suggested that the termination of a glacial period is first marked by a decrease in the rate of formation or even stagnation of bottom waters (this would result in an increase in dissolved carbon dioxide in the bottom waters, leading to accelerated carbonate dissolution). He further suggests that the bottom water stagnation would be succeeded by reduced upwelling (leading to reduced opal deposition) and finally by wasting of continental glaciers. The data from core Y69-106P are in complete accord with Newell's model. If confirmed by data from other geographical areas, these results support continued development of the model and seem capable of providing accurate estimates of the lag times involved in the change of the oceanic and cryospheric systems from glacial to interglacial modes.

This research was supported by the National Science Foundation. We thank N. J. Shackleton and W. H. Berger for comments and criticisms.

NICKLAS G. PISIAS
G. ROSS HEATH
TED C. MOORE, JR

Graduate School of Oceanography, University of Rhode Island, Kingston, Rhode Island 02881

Received October 29, 1974; accepted July 16, 1975.

1 McIntyre, A., Ruddiman, W. F., and Jantzen, R., *Deep-Sea Res.*, **19**, 61-77 (1972).
2 Shackleton N. J., and Opdyke, N., *Quat. Res.*, **3**, 39-55 (1973).
3 Berger, W. H., *J. foram. Res.*, **3**, 187-195 (1973).
4 Thompson, P. R., and Saito, T., *Geology*, **2**, 333-338 (1974).
5 Arrhenius, G., *Swedish Deep-sea Expeditions* (1947-1948) *Reports*, **5**, 89 p. (1952).
6 Hays, J. D., Saito, T., Opdyke, N. D., and Burckle, L. H., *Geol. Soc. Am. Bull.*, **80**, 1481-1514 (1969).
7 Luz, B. and Shackleton, N. J., *Cushman Found. Foram. Res. Spec. Pub.*, **13**, 142-150 (1974).
8 Newell, R. E., *Quat. Res.*, **4**, 117-127 (1974).
9 Molina-Cruz, A., thesis, Oregon State Univ. (1975).
10 Pisias, N. G., with appendix by Shackleton, N. J., *Geol. Soc. Am. Spec. Pap.* (in the press).
11 Broecker, W. S., Turekian, K. K., and Heezen, B. C., *Am. J. Sci.*, **256**, 503-517 (1958).
12 Heath, G. R., *Paleo-oceanography: SEPM Special Pub.*, **20**, 77-93 (1974).
13 Weyl, P. K., *Meteorol. Monogr.*, **8**, 37-62 (1968).

Strain resulting from adhesive action of water in capillary bridges

WE report here on the measurement of adhesive forces of thin films of water between glass plates. Our approach differed from the traditional method of measuring the force necessary to rupture the liquid film in tension[1-3]; we used interferometry to measure the elastic strains produced around the bridges. The main pupose of the study was to assess the degree of agreement between measured adhesive forces and those predicted by classical capillary theory.

When a surface-energy consideration is applied to a liquid bridge between a deformable capillary wall and a rigid capillary wall, the work done by the force F during an increase, db, in the distance b (Fig. 1) is equal to the energy of wetting and the elastic bending energy of the capillary wall:

$$F\mathrm{d}b = (\gamma_{SV}-\gamma_{SL})\mathrm{d}A_{SL}+\gamma_{LV}\,\mathrm{d}A_{LV}+\mathrm{d}U \qquad (1)$$

where γ is an interfacial energy, A an interfacial area, and the subscripts S, V and L denote solid, vapour and liquid, respectively; U is the bending energy in the capillary wall. From the Young–Dupre equation, $\gamma_{LV}\cos\theta$ can be substituted for $(\gamma_{SV}-\gamma_{SL})$ with θ being the contact angle of the liquid on the

Fig. 1 Displacement, db, in a deformable isolated capillary. (From surface-energy considerations.)

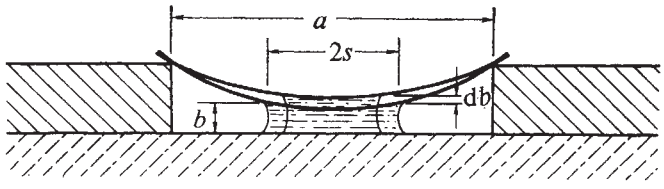

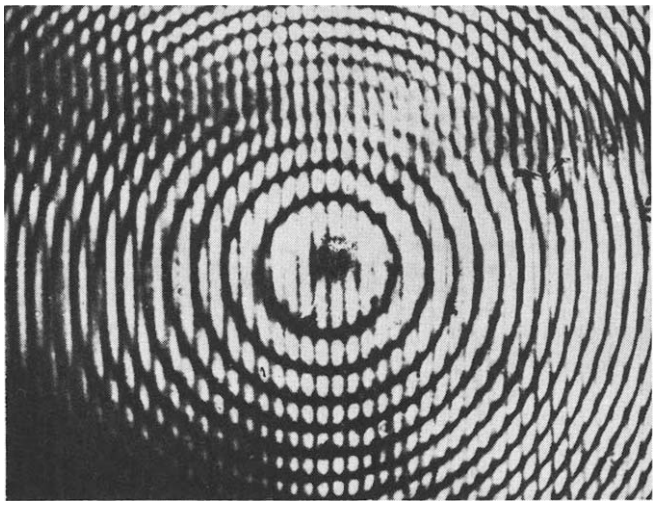

Fig. 2 Interference fringe pattern obtained by a mechanical loading of 20,482 dyne.

Fig. 3 Interference fringe pattern obtained by capillary adhesion. An adhesive force of 9,510 dyne is measured.

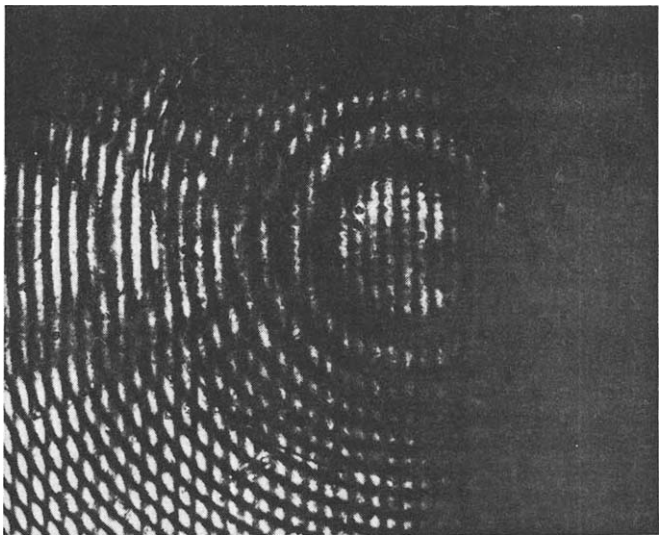

capillary wall. The theory of bending of plates[4] gives:

$$dU = Fdb/\cos(s\pi/a) \quad (2)$$

When $s \gg b$, the term $\gamma_{LV}dA_{LV}$ is negligible, and by using β to represent $s\pi/a$ equations (1) and (2) can be combined to give

$$\frac{F}{\pi s^2}(1 + \frac{1}{\cos\beta}) = \gamma\cos\theta\frac{2}{b}, \quad (3)$$

which indicates a linear relationship with a slope of $\gamma\cos\theta$.

A helium–neon laser beam was directed normal to two parallel glass capillary walls separated by a metal spacer 2 μm thick. Deflections of the deformable wall under applied forces gave rise to interference fringe patterns which are linearly related to the magnitudes of the applied forces. Mechanical loading was used to produce fringe patterns for calibration (Fig. 2).

Fringe patterns were obtained with water bridges having diameters of 0.04, 0.070, 0.12 and 0.13 cm (Fig. 3). Next, the forces of adhesion were calculated based on the calibration.

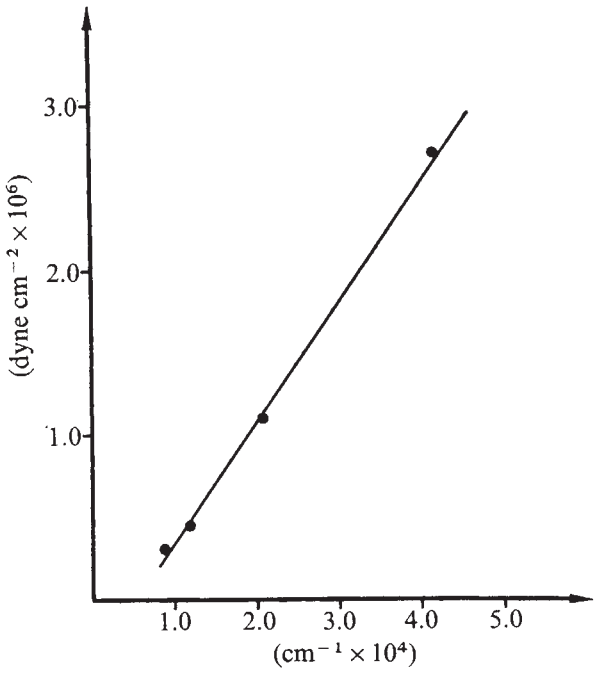

Fig. 4 The relationship of $(F/\pi s^2)(1+1/\cos\beta)$ (ordinate) and $2/b$ (abscissa) for a deformable glass–water capillary system. The experimental value of $\gamma\cos\theta$ is 73.9 dyne cm^{-1}, compared with a predicted value of 72 dyne cm^{-1}.

Using these results, Fig. 4 was plotted. The slope of the linear regression line is 73.9 dyne cm^{-1} which, from equation (3), would be equal to γ since θ was near zero. This close agreement with the surface tension value of water supports the correctness of equation (3). The results indicate that the surface energy of wetting can account for the elastic strains observed.

This work was supported by grants from the National Institute of Dental Research.

P. L. Fan
W. J. O'Brien

University of Michigan,
Ann Arbor, Michigan 48104

Received June 16; accepted July 9, 1975.

1 McFarlane, J. S., and Tabor, D., *Proc. R. Soc.*, **A202**, 224–243 (1950).
2 O'Brien, W. J., and Yu, C. U., *Surf. Sci.*, **32**, 739–742 (1972).
3 O'Brien, W. J., and Hermann, J. J., *J. Adhes.*, **5**, 91–103 (1973).
4 Timoshenko, S., *Theory of Elastic Stability*, 314–316 (McGraw-Hill, New York, 1936).

Three-coordinated magnesium in dehydrated offretite

Offretite is a rare natural zeolite whose synthetic equivalent, zeolite O, is commercially important as a molecular sieve[1]. Its aluminosilicate framework is topologically related to that of erionite[2], an abundant natural zeolite[3]. The catalytic properties of molecular sieve zeolites have been ascribed to framework-bound protons, strong electrostatic fields, and oxygen vacancies in the framework[4]. As befits the small radius of Mg^{2+} ions (0.049 nm for four-coordination, 0.072 for six-coordination and 0.089 for eight-coordination)[5], Mg normally occurs in six-coordination with oxygen and hydroxyl, though four, five and eight-coordinations occur infrequently (for example, four-akermanite: $Ca_2MgSi_2O_7$, Mg–O = 0.1876 nm; five-grandidierite: $(Mg,Fe)Al_3O.BO_4.SO_4$, 0.2176, 0.2054, 0.2040, 2×0.1970; farringtonite: Mg_3PO_4, 0.196, 0.197, 0.201, 0.206, 0.214; eight-pyrope: $Mg_3Al_2Si_3O_{12}$, 4×0.2196, 4×0.2342)[6]. We report here on the occurrence of three-coordinated Mg in dehydrated offretite, which should produce a strong electrostatic effect on adjacent sorbed molecules.

Table 1 Atomic coordinates

	x/a	*y/b*	*z/c*
Si(1)*	0.9998(3)	0.2277(2)	0.2177(2)
Si(2)	0.0968(3)	0.4273(3)	0.5
O(1)	0.0408(6)	0.3511(5)	0.3182(9)
O(2)	0.0896(3)	0.9104(3)	0.2783(10)
O(3)	0.8722(9)	0.1278(4)	0.2879(11)
O(4)	0.0030(9)	0.2483(7)	0
O(5)	0.2425(6)	0.7575(6)	0.5
O(6)	0.4592(7)	0.5408(7)	0.5
Ca	0	0	0.5
K	0.4964(12)	0.5036(12)	0
Mg	0.333	0.667	0.5

*Numbers in brackets are atom designation numbers.

Hydrated offretite[7] ($K_{1.1}Ca_{1.1}Mg_{0.7}Si_{12.8}Al_{5.2}O_{36}.15H_2O$) contains a K ion in each cancrinite cage, a pentahydrate of Mg in each gmelinite cage, and hydrated Ca ions in the main channels. Electron microprobe analysis of a new crystal, from Mount Simiouse, France, showed that this had $K_{1.04}Ca_{1.04}Mg_{0.95}Al_{5.2}Si_{12.8}O_{36}$ atoms in each cell. The crystal was dehydrated in a silica capillary for 22 h at 500 °C and 10^{-5} torr before sealing. Using MoKα radiation, 4,700 intensity measurements at room temperature yielded 514 independent non-zero diffractions in P$\bar{6}$m2, *a* 1.3229(5), *c* 0.7338(4) nm. Least-squares refinement yielded the coordinates shown in Table 1.

The stereo plot (Fig. 1) shows Mg occupying the centre of a single six-ring where it is bonded to three oxygens at 0.208(1) nm. The six-ring is very distorted to accommodate this short distance and the other three oxygens are displaced outwards to 0.288(2) nm. Some weak bonding may occur to these three oxygens, but the strong disparity in the distances implies that the Mg is effectively three-coordinated. Each Ca ion lies between two six-rings which are distorted so that three oxygens from each give near-octahedral coordination at 0.2619(8) nm. Each K ion lies at the middle of a distorted eight-ring with four oxygens at 0.3258(7) as nearest neighbours and two more at 0.3350(6) nm. All the cation–oxygen distances are longer than the values expected from simple ionic theory and distances found in most silicates (for instance, Ca–O = 0.24; K–O = 0.27; and predicted Mg–O for three-coordination is less than 0.19 nm). The mean Al, Si–O distance of 0.1631 nm is less than the value of 0.165 obtained by interpolating the Al/Si ratio of offretite between the data for anhydrous framework silicates[8]. This suggests that the bonding in the framework of the dehydrated zeolite is stronger than in normal silicates and that the bonding